Electron Photodetachment of the Phenylnitrene Anion Radical: EA, $\Delta H°_f$, and the Singlet–Triplet Splitting for Phenylnitrene

Richard N. McDonald* and Stephen J. Davidson

Contribution from the Department of Chemistry, Kansas State University, Manhattan, Kansas 66506

Received July 30, 1992. Revised Manuscript Received February 9, 1993

Abstract: The electron photodetachment (0,0) transitions from the $^2B_2$ ground electronic state of $PhN^{\bullet-}$ to the ground triplet state, $^3A_2$, and the excited singlet state, $^1A_2$, of PhN are observed in the relative photodetachment cross section vs wavelength spectrum of $PhN^{\bullet-}$ between 540 and 920 nm. The (0,0) transition thresholds are determined at 867.9 ± 7 nm (1.429 ± 0.011 eV) for $^3A_2$ PhN and 557.6 ± 7 nm (2.224 ± 0.028 eV) for the $^1A_2$ excited state, which are the respective electron affinities of the these two electronic states of PhN. From these values, the singlet–triplet splitting energy for PhN of 0.795 ± 0.030 eV (18.33 ± 0.69 kcal mol^{-1}) is measured. The (0,0) feature of $^3A_2$ PhN is followed by three additional features that are part of a vibrational progression (average spacing 476 cm^{-1}) of triplet PhN. The more intense (0,0) feature of $^1A_2$ PhN is preceded by a two component hot band progression. Based on $\Delta H°_{f,298}(^2B_2$ $PhN^{\bullet-}) = 62.9 \pm 4.3$ kcal mol^{-1}, $\Delta H°_{f,298}(^3A_2$ PhN) = 95.9 ± 4.3 kcal mol^{-1} and $\Delta H°_{f,298}(^1A_2$ PhN) = 114.2 ± 4.3 kcal mol^{-1} are obtained.

Introduction

The monovalent, nitrogen-centered reactive intermediate phenylnitrene (PhN) has been the subject of considerable interest over the years.[1] Access to this species has generally involved thermolysis or photolysis of phenyl azide and, less frequently, phenyl isocyanate by analogy to the formation of divalent carbenes from similar treatment of diazo or diazirene compounds and ketenes.[2] By analogy with the carbenes, the initially generated PhN will be in its singlet excited state, $^1A_2$, and must undergo intersystem crossing to yield the triplet ground electronic state, $^3A_2$. PhN and several other nitrenes were previously determined by Smolinsky et al.[3a] to have triplet ground states using EPR of rigid glasses at 77 K.

The varied rearrangements reported for PhN,[1,4] while at first confusing, have now been relegated to conventional processes defined by the internal energy of the singlet PhN intermediate, which depends on the experimental conditions. The Platz–Miller scheme[4f,g] describing these rearrangements is shown in Scheme I. The rearrangement competitive with intersystem crossing to $^3A_2$ PhN in fluid solution at ambient temperature is ring expansion of **1** to azacycloheptatetraene (**2**). In the gas phase, UV photolysis is usually employed (excimer laser line 248 nm, 115 kcal mol^{-1}) and the competing rearrangement is ring contraction to the global energy minimum, cyanocyclopentadiene (**3**). Thus, the extent of

Scheme I

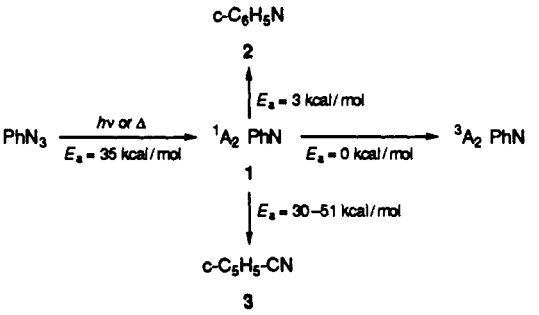

$^3A_2$ PhN generation is controlled by the energy content of the singlet PhN precursor and the efficiency of the intersystem crossing compared to the **1** → **2** and the **1** → **3** rearrangements. Only in frozen glasses and rare gas matrices can the rearrangement steps be eliminated.[5]

An alternate approach to specifically generate $^3A_2$ PhN is to photodetach an electron from the $^2B_2$ ground electronic state of $PhN^{\bullet-}$ ions[6] by using photons of the proper energy. Although this approach is not practical for most chemical studies, the general procedure outlined in eq 1 is used to accurately measure the

$$M^- + h\nu \rightarrow M + e^- \quad (1)$$

electron affinities (EA) of neutral molecules, M, formed from the corresponding negative ions, M^-, in the gas phase. The two methods most widely used today to achieve this result are photoelectron spectroscopy (PES) and electron photodetachment (EPD). Both methods have the ability to probe excited vibrational and electronic states of the neutral and the anion. The EPD method uses a tunable light source, either a conventional lamp–monochrometer source or a laser system. The gas-phase apparatus includes ion cyclotron resonance (ICR) spectrometers,[7] high-

(1) Early reviews of nitrenes, their structures, and rearrangements include the following: (a) Horner, L.; Christmann, A. *Angew. Chem., Int. Ed. Engl.* **1963**, *2*, 599. (b) Lwowski, W., Ed. *Nitrenes*; Wiley-Interscience: New York, 1970. (c) Wentrup, C. *Top. Curr. Chem.* **1976**, *62*, 173. (d) Wentrup, C. *Reactive Molecules*; Wiley-Interscience: New York, 1984. (e) Platz, M. S. In *Azides and Nitrenes*; Scriven, E. F. V., Ed.; Academic Press: New York, 1984; Chapter 7.

(2) For example, see: Moss, R. A.; Jones, M., Eds. *Carbenes*; Wiley-Interscience: New York, 1973, Vol. 1; 1975, Vol. 2.

(3) (a) Smolinsky, G.; Wasserman, E.; Yager, W. A. *J. Am. Chem. Soc.* **1962**, *84*, 3220. (b) Yager, W. A.; Wasserman, E.; Cramer, R. M. R. *J. Chem. Phys.* **1962**, *37*, 1148.

(4) (a) Porter, G.; Ward, B. *Proc. R. Soc. A* **1968**, *303*, 139. (b) Chapman, O. L.; Sheridan, R. S.; Leroux, J. P. *J. Am. Chem. Soc.* **1978**, *100*, 6245. (c) Leyva, E.; Platz, M. S. *Tetrahedron Lett.* **1985**, *26*, 2147. (d) Leyva, E.; Platz, M. S.; Persy, G.; Wirz, J. *J. Am. Chem. Soc.* **1986**, *108*, 3783. (e) Li, Y.-Z.; Kirby, J. P.; George, M. W.; Poliakoff, M.; Schuster, G. B. *J. Am. Chem. Soc.* **1988**, *110*, 8092. (f) Cullin, D. W.; Soundararajan, N.; Platz, M. S.; Miller, T. A. *J. Phys. Chem.* **1990**, *94*, 8890. (g) Young, M. J. T.; Platz, M. S. *J. Org. Chem.* **1991**, *56*, 6403.

(5) The reader is referred to ref 4f for a discussion of the relevant parts of Scheme I and, especially, the assignment of cyanocyclopentadiene as the gas-phase product.

(6) Travers, M. J.; Cowles, D. C.; Clifford, E. P.; Ellison, G. B. *J. Am. Chem. Soc.* **1992**, *114*, 8699.

0002-7863/93/1515-10857$04.00/0

pressure drift tubes[8,9] and flowing afterglows,[10] and crossed-beam[11,12] and coaxial ion-laser beams.[13-15]

Dissociative electron attachment to PhN_3 cleanly yields large ion signals of $PhN^{\bullet-}$ at m/z 91 (eq 2). Some important thermo-

$$PhN_3 + e^- \rightarrow \underset{m/z\ 91}{PhN^{\bullet-}} + N_2 \qquad (2)$$

dynamic values (proton affinity (PA) = 371.9 ± 3.8 kcal mol^{-1},[16,17] $\Delta H^\circ_{f,298}$ = 62.9 ± 4.3 kcal mol^{-1})[21] and chemistry[16,23,24] of this interesting anion radical have been reported. Chemically, $PhN^{\bullet-}$ exhibits (i) poor nucleophilic character in S_N2 displacement reactions,[23c,23e,24] (ii) variable reactivity with carbonyl-containing organic molecules ($k_{C=O}$, RCHO > $R_2C{=}O$ > RCO_2R'),[23c,23e] and (iii) high regioselectivity toward addition/fragmentation at the carbonyl group in α,β-unsaturated carbonyl substrates.[23b,23d]

The EPD of $PhN^{\bullet-}$ was reported in 1984; an ICR with a xenon arc lamp and monochrometer as the light source was used.[19,25] Three thresholds were observed at 848 ± 8, 752 ± 8, and 672 ± 8 nm and were assigned to the (0,0) transitions yielding the ground triplet state and the first two excited singlet states of PhN, respectively. The reported energy splittings between the ground triplet state and the two excited singlet states of PhN were 4.3 ± 0.4 and 8.8 ± 0.5 kcal mol^{-1}.

Two developments caused us to question these results. First, during the testing of our flowing afterglow/laser system[10] in 1987, $PhN^{\bullet-}$ was examined briefly as an negative ion substrate. We expected to observe considerable photodestruction of $PhN^{\bullet-}$ with ≈600 nm photons based on the reported sharply rising EPD relative cross section with its origin at 848 nm.[19,25] Observation of <10% photodestruction of the negative ions at 585 nm with ≈40 W intracavity photon power, the single wavelength examined at that time, suggested that the photodetachment relative cross section at this wavelength was different from that reported. The second development was a request by Professor M. S. Platz in 1989 that we reexamine the EPD of $PhN^{\bullet-}$ because the electronic state splittings reported for PhN were not in agreement with theory.[4e,26] The recent theoretical[27,28] and PES[6,29] reports of the singlet–triplet gap for PhN of ≈18 kcal mol^{-1} support this concern.

The results and interpretations of a reinvestigation of the $PhN^{\bullet-}$ photodetachment yielding an experimental PhN triplet–singlet energy gap of 18.33 ± 0.69 kcal mol^{-1} are the subject of this paper.

Experimental Section

The flowing afterglow/laser system (FA/L) used in this study has been described in detail elsewhere.[10] The $PhN^{\bullet-}$ ions (m/z 91) were generated in the upstream end of the FA flow tube in a fast flow of helium buffer gas (P_{He} = 1.0 Torr, v = 46 m s^{-1}, 298 K; [He] ≈ 3 x 10^{16} atoms cm^{-3}) according to eq 2. The PhN_3 addition port was located 140 cm upstream from the first ion sampling nose cone and 6 cm downstream of the electron gun (thorium oxide coated iridium filament) operated at a low (20–30 μA) emission current. With these conditions, the final 65 cm of the flow was shown to be free of electrons and metastable He(2^3S) atoms by the addition of SF_6 to the flow (see below) and the absence of the formation of $SF_6^{\bullet-}$ ions; the relevant equations are (i) $SF_6 + e^- \rightarrow SF_6^{\bullet-}$ (m/z 146) and (ii) $SF_6 + He(2^3S) \rightarrow [SF_6^{\bullet-} + e^- + He$[30] followed by (i).

The addition of PhN_3 was carefully controlled to eliminate formation of the secondary ion products $PhN{=}NPh^{\bullet-}$ (m/z 182) and $PhN{=}N{-}N{=}NPh^{\bullet-}$ (m/z 210) produced by the slow reaction of $PhN^{\bullet-}$ with excess PhN_3.[16] It was determined that both of these secondary ions are photoactive in the wavelengths used in the EPD experiment. Under the above conditions, *the $PhN^{\bullet-}$ ions* (m/z 91 and its 7% naturally occurring isotope peak at m/z 92 at greater than unit mass resolution) *were the only negative ions observed in the 10–300 amu range.*

The $PhN^{\bullet-}$ ion containing flow was sampled via two nose cones into a differentially pumped compartment containing the quadrupole mass filter and multiplier, which continuously monitored the ion composition in the flow. During the EPD experiments, the mass filter was operated in the single ion mode. The laser system uses the output of a continuous wave (CW) argon ion laser to pump a tunable dye laser. The dyes presently available with sufficient efficiency for our purposes cover the wavelength range of 540–920 nm.

For the EPD runs made with each dye, approximately (1–4) × 10^{13} molecules cm^{-3} of SF_6 was added via an inlet port located 75 cm downstream of the PhN_3 inlet and 65 cm upstream from the first ion sampling nose cone. SF_6 was added to the $PhN^{\bullet-}$ ion containing flow to attach the photoelectrons produced in the EPD experiment; no reaction was observed between $PhN^{\bullet-}$ and SF_6. With the laser-off cycle, *no* $SF_6^{\bullet-}$ ion counts were observed above the instrument background measured at m/z 144–150 in the presence or absence of added SF_6. Thus, the initially formed excited $PhN^{\bullet-}$ ions, on the average, undergo >10^5 collisions with the helium buffer gas and >100 collisions with the polynuclear SF_6 molecules as the ions traverse the ≈1.4 m length of the flow tube before interacting with the photon beam. We conclude that the $PhN^{\bullet-}$ ions undergoing EPD are thermalized.

The extended cavity of the dye laser includes a cross section of the FA with the ≈2 mm diameter photon beam passing just in front of the 1 mm orifice of the first ion-flow sampling nose cone. With laser-on and laser-off cycles supplied by a chopper, the changes in the ion counts as a function

(7) For example, see: (a) Janousek, B. K.; Brauman, J. I. In *Gas Phase Ion Chemistry*; Bowers, M. T., Ed.; Academic Press: New York, 1979; Vol. 2, Chapter 10. (b) Drzaic, P. S.; Marks, J.; Brauman, J. I. In *Gas Phase Ion Chemistry: Ions and Light*; Bowers, M. T., Ed.; Academic Press: New York, 1984; Vol. 3, Chapter 21.

(8) Woo, S. B.; Helmy, E. M.; Mauk, P. H.; Paszek, A. P. *Phys. Rev.* **1981**, *64*, 1380.

(9) Moseley, J. T. In *Applied Atomic Collision Physics*; Massey, H. S. W., McDaniel, E. W., Bederson, B., Eds.; Academic Press: New York, 1982; Vol. 5, p 269.

(10) McDonald, R. N.; Bianchina, E. J.; Tung, C. C. *J. Am. Chem. Soc.* **1991**, *113*, 7115.

(11) Slater, J.; Read, F. H.; Novick, S. E.; Lineberger, W. C. *Phys. Rev. A* **1978**, *17*, 201.

(12) Jones, P. L.; Mead, R. D.; Kohler, B. E.; Rosner, S. D.; Lineberger, W. C. *J. Chem. Phys.* **1980**, *78*, 4419.

(13) Moseley, J. T.; Durup, J. *Annu. Rev. Phys. Chem.* **1981**, *32*, 53.

(14) Hefter, U.; Mead, R. D.; Schulz, P. A.; Lineberger, W. C. *Phys. Rev. A* **1983**, *28*, 1429.

(15) Carrington, A.; Kennedy, R. A. In *Gas Phase Ion Chemistry*; Bowers, M. T., Ed.; Academic Press: New York, 1984; Vol 3, Chapter 26.

(16) McDonald, R. N.; Chowdhury, A. K.; Setser, D. W. *J. Am. Chem. Soc.* **1981**, *103*, 6599. The PA bracketing of $PhN^{\bullet-}$ was achieved with CH_3CN (3% H^+ transfer observed accompanied by 23% H-atom transfer;[17] ΔH°_{acid} = 372.8 ± 2.4 kcal mol^{-1})[20] and $(CH_3)_2SO$ (no reaction observed, k < 10^{-13} cm^3 molecule^{-1} s^{-1}; ΔH°_{acid} = 373.6 ± 2.6 kcal mol^{-1})[20] with the revised gas-phase acidities.[20] The small rate constant (3.2 × 10^{-11} cm^3 molecule^{-1} s^{-1}) for the overall complex reaction of $PhN^{\bullet-}$ with CH_3CN and the very small H^+ transfer branching fraction suggesting equilibrium H^+ transfer between the reactants lead us to conclude that $PA(PhN^{\bullet-}) \leq PA(NCCH_2^-)$. Thus, the value of $PA(PhN^{\bullet-})$ = 371.9 ± 3.8 kcal mol^{-1} suggested in ref 20 is adopted here.

(17) Considering the transfer complex as the ternary structure [$PhNH^{\bullet}$/$^{\bullet}CH_2CN$/e^-], the reason for the small ratio of the branching fractions for H^+ vs H-atom transfer in the reaction of $PhN^{\bullet-}$ with CH_3CN lies in the EAs of the two organic radicals, $EA(^{\bullet}CH_2CN)$ = 1.543 ± 0.014 eV[18] and $EA(PhNH^{\bullet})$ = 1.70 ± 0.03 eV.[19]

(18) Moran, S.; Ellis, H. B.; DeFrees, D. J.; McLean, A. D.; Ellison, G. B. *J. Am. Chem. Soc.* **1987**, *109*, 5996.

(19) Drzaic, P. S.; Brauman, J. I. *J. Phys. Chem.* **1984**, *88*, 5285.

(20) Lias, S. G.; Bartmess, J. E.; Liebman, J. F.; Holmes, I. L.; Levin, R. D.; Mallard, W. G. *J. Phys. Chem. Ref. Data* **1988**, *17*, Suppl. 1.

(21) Using $\Delta H^\circ_f(PhNH^{\bullet})$ = 56.7 ± 2 kcal mol^{-1} [22] and $\Delta H^\circ_f(H^+)$ = 365.7 kcal mol^{-1} with the ion "stationary electron" convention.[20]

(22) McMillen, D. F.; Golden, D. M. *Annu. Rev. Phys. Chem.* **1982**, *33*, 493.

(23) (a) McDonald, R. N.; Chowdhury, A. K. *J. Am. Chem. Soc.* **1980**, *102*, 5118. (b) McDonald, R. N.; Chowdhury, A. K. *J. Am. Chem. Soc.* **1980**, *102*, 6146. (c) McDonald, R. N.; Chowdhury, A. K. *J. Am. Chem. Soc.* **1981**, *103*, 674. (d) McDonald, R. N.; Chowdhury, A. K. *J. Phys. Chem.* **1982**, *86*, 3641. (e) McDonald, R. N.; Chowdhury, A. K. *J. Am. Chem. Soc.* **1983**, *105*, 198.

(24) Pellerite, M. J.; Brauman, J. I. *J. Am. Chem. Soc.* **1981**, *103*, 676.

(25) Drzaic, P. S.; Brauman, J. I. *J. Am. Chem. Soc.* **1984**, *106*, 3443.

(26) Ishida, T.; Abe, H.; Nakajima, A.; Kaya, K. *Chem. Phys. Lett.* **1990**, *170*, 425.

(27) Kim, S.-J.; Hamilton T. P.; Schaefer, H. F. *J. Am. Chem. Soc.* **1992**, *114*, 5349.

(28) Hrovat, D. A.; Waali, E. E.; Borden, W. T. *J. Am. Chem. Soc.* **1992**, *114*, 8698.

(29) We thank Professor Ellison for communicating the preliminary PES spectrum and threshold data in 1991.

(30) Jones, M. T.; Dreiling, T. D.; Setser, D. W.; McDonald, R. N. *J. Phys. Chem.* **1985**, *89*, 4501.

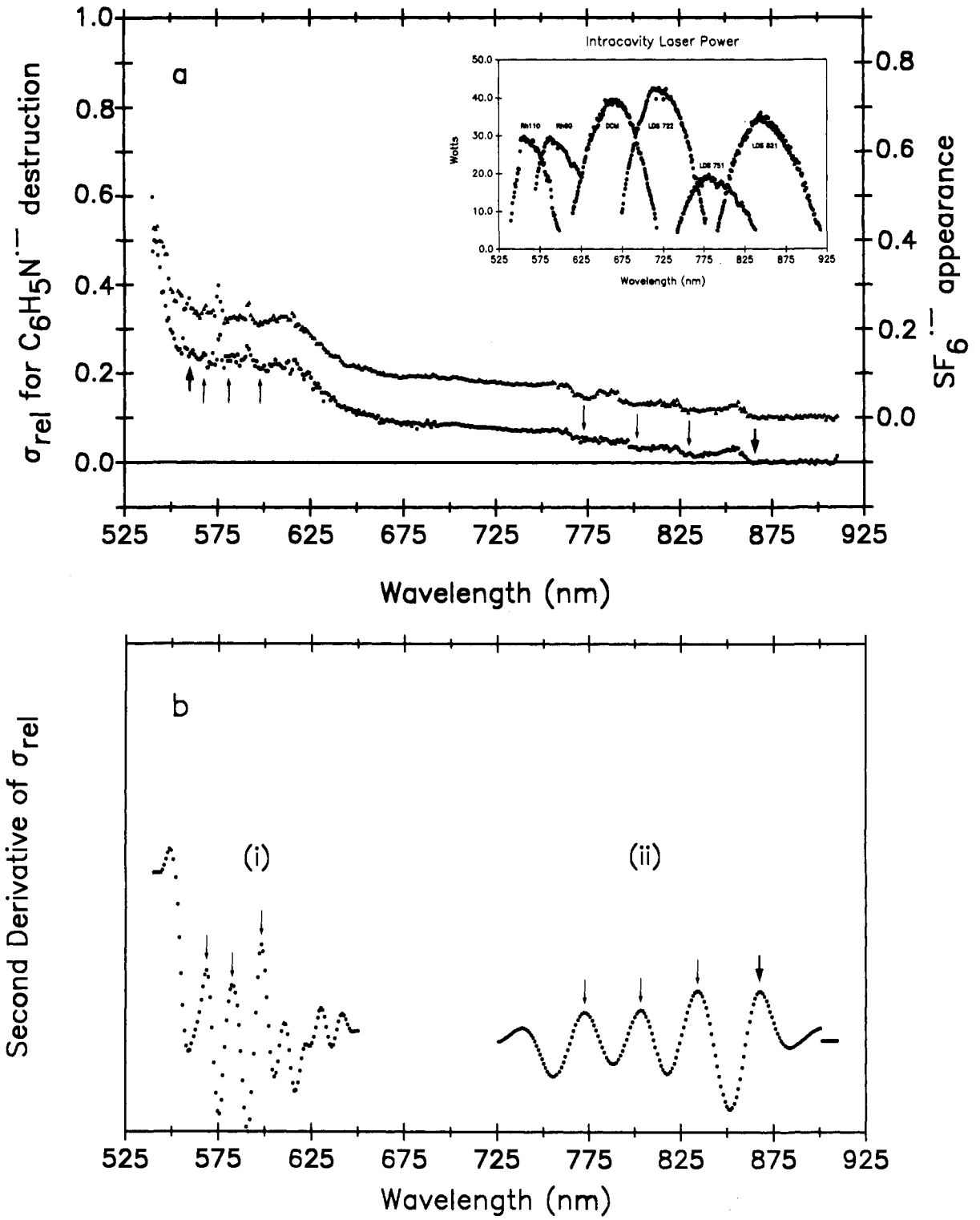

Figure 1. (a) Plot of the relative cross section vs wavelength electron photodetachment spectrum of $PhN^{\cdot-}$ (left vertical axis) and appearance of $SF_6^{\cdot-}$ vs wavelength (offset right vertical axis). The plateau at ≈620 nm has been shown to be an artifact from folding together the Rh6G and DCM dye data sets. (b) Plot of the second derivative of smoothed data of Figure 1a. In both (a) and (b), thresholds are marked with arrows; (0,0) thresholds are shown with bold arrows. The wavelengths for joining the dye data sets are 804, 757, 701, 621, and 581 nm.

of wavelength are measured. The noise level of the FA/L is low and allows changes in the large ion signals (typically $\geq 5 \times 10^5$ ions s^{-1}) of <0.06% to be observed. The experimental reproducibility of thresholds or other features is generally ±3 nm.

The workup of the laser-on ion count data is normalized for the photon flux variations at the different wavelengths of the particular dye in use. The voltage output from a power meter monitoring a reflection from the rear Brewster angle quartz window on the FA is used in this normalization.

To establish the photodetachment as a one-photon process, the percentage of EPD ($(I_0 - I)/I_0$; see eq 3 for symbol descriptions) as a function of the intracavity photon power was determined at a single wavelength for each dye. The linear relationship with unit slope obtained from the ln–ln plots of these two functions ruled out any higher order process throughout the wavelength range examined.

Results

The relative cross section (σ_{rel}) vs wavelength EPD spectrum for $PhN^{\cdot-}$ is shown in Figure 1a as the lower curve associated with the left vertical axis. The σ_{rel} for $PhN^{\cdot-}$ photodestruction

are calculated by eq 3 where I_0 and I are the average $PhN^{\bullet-}$ ion

$$\sigma_{rel} = \frac{\log(I_0/I)}{\Phi(\lambda)} \quad (3)$$

counts at a given wavelength for the laser-off and laser-on periods, respectively, and $\Phi(\lambda)$ is the photon flux at that wavelength. The power curves for the six dyes (Rh110, Rh6G, DCM, LDS 722, LDS 751, and LDS 821) are given in the insert in Figure 1a and are used in the laser-on ion count data normalization. Data points are measured at 1-nm intervals. The individual data sets for the dye runs are then folded together[31] starting at the low-energy end of the wavelength scale where $\sigma_{rel} = 0$ for photodestruction of $PhN^{\bullet-}$ within our error limits.

When the EPD data set for a particular dye was completed, the mass filter was reset to pass only the $SF_6^{\bullet-}$ ions at m/z 146 ± 3 and the experiment was repeated to follow $SF_6^{\bullet-}$ ion appearance. The $SF_6^{\bullet-}$ ions at m/z 146 are formed by capture of the photodetached electrons from EPD of $PhN^{\bullet-}$ by SF_6 ($\approx 10^{13}$ molecules cm^{-3}) present in the flow. The upper offset curve with the right vertical axis in Figure 1a is the $SF_6^{\bullet-}$ ion appearance vs wavelength data treated in the form of a cross section of a daughter ion to allow for direct comparison with σ_{rel} of $PhN^{\bullet-}$ photodetachment. The appearance of $SF_6^{\bullet-}$ is calculated according to eq 4

$$\text{appearance of } SF_6^{\bullet-} = \frac{\log(I_0/(I_0 - (I_D - I_{0,D})))}{\Phi(\lambda)} \quad (4)$$

where $I_{0,D}$ (corrected for background ion counts at this mass) and I_D are the $SF_6^{\bullet-}$ ion counts obtained during the laser-off and laser-on periods, respectively; I_0 and $\Phi(\lambda)$ have the same meaning as in eq 3. Very similar I_0 values in eq 4 ($PhN^{\bullet-}$ ion counts) were obtained at the beginning and end of the runs measuring the appearance of $SF_6^{\bullet-}$. In Figure 1a, the two curves track each other quite well, and the $SF_6^{\bullet-}$ ion counts represent >90% of the photodisappearance of the $PhN^{\bullet-}$ ion counts over this entire wavelength range. It was established separately with each dye used that the presence or absence of SF_6 in the flow containing $PhN^{\bullet-}$ had no effect on the σ_{rel} for EPD of $PhN^{\bullet-}$.

To determine the thresholds of the features in Figure 1a marked by the arrows, the data are smoothed and first and second derivatives are obtained of the smoothed data set.[10,32] This method of resolving EPD spectra was introduced by Janousek et al.[33] and used in our previous work.[10] Because the low-energy features are larger and are defined by greater than twice the number of data points as the high-energy features, the two regions were smoothed separately and the separate derivatives were taken. The composite second derivative is shown in Figure 1b. The wavelengths of the thresholds in parts a and b of Figure 1 were read from the computer data for the second derivative.

A total of seven runs were carried out with Rh110 on different days while 8–12 separate runs were made with each of the other dyes. Each of these runs required minor laser realignment and adjustments of the extended cavity for optimization of the mode and power. In all runs, the features shown for each dye in Figure 1 were observed with a maximum deviation of ±3 nm in the features average λ_{max} and thresholds. Taking into account the additional uncertainties, e.g. the monochrometer (±0.5 nm), the stepper motor, etc., we suggest the reasonable estimated error limits of ±7 nm for these results.

Discussion

For $PhN^{\bullet-}$, the $^2B_2$ state with the electron pair and the spin unpaired electron in b_1 and b_2 orbitals, respectively, is calculated to be the ground state, ≈10 kcal mol^{-1} lower in energy than the $^2B_1$ state.[6] The partial electron configuration of $^2B_2$ $PhN^{\bullet-}$ is shown below along with those of the triplet ground state ($^3A_2$), the first triplet excited state ($^3B_1$), and the two lowest energy singlet states ($^1A_2$ and $^1A_1$) of PhN. The orbital assignments for PhN are those given by Kim et al. in structure **1**;[27] the $2b_1$ and $1a_2$ orbitals are π_2 and π_3, respectively, of the ring.

$^2B_2$ $PhN^{\bullet-}$ $\ldots(13a_1)^2(2b_1)^2(1a_2)^2(3b_1)^2(8b_2)^1$

$^3A_2$ and $^1A_2$ PhN $\ldots(13a_1)^2(2b_1)^2(1a_2)^2(8b_2)^1(3b_1)^1$

$^1A_1$ PhN $\ldots(13a_1)^2(2b_1)^2(1a_2)^2(8b_2)^2$

$^3B_1$ PhN $\ldots(13a_1)^2(2b_1)^2(1a_2)^1(8b_2)^1(3b_1)^2$

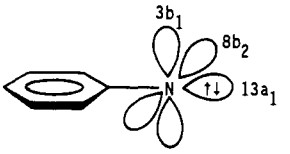

1

Detaching an electron from the doubly-occupied $3b_1$ orbital of $^2B_2$ $PhN^{\bullet-}$ yields the *open-shell* $^3A_2$ or $^1A_2$ PhN species; the spins of the unpaired electrons in the $^1A_2$ state of PhN are antiparallel with the same electronic configuration as the triplet ground state. Both conversions are allowed one-electron photodetachment processes. The corresponding $^1A_1$ PhN ← $^2B_2$ $PhN^{\bullet-}$ conversion is not an allowed photodetachment process and, further, the energy of the $^1A_1$ state lies 14 kcal mol^{-1} above that of the $^1A_2$ state.[27] Although the $^3B_1$ PhN ← $^2B_2$ $PhN^{\bullet-}$ photodetachment is allowed, detaching an electron from the ring π_3 orbital requires more energy; the adiabatic excitation from the ground state $^3A_2$ PhN to the $^3B_1$ excited state is 53 kcal mol^{-1}.[27] The previously reported 848 nm (1.46 eV) EPD[19,25] and 1.45 eV PES[6] (0,0) thresholds for the $^3A_2$ PhN ← $^2B_2$ $PhN^{\bullet-}$ detachment and the ≈18 kcal mol^{-1} $^3A_2$–$^1A_2$ energy gap in PhN[6,27,28] predict the $^1A_2$ PhN ← $^2B_2$ $PhN^{\bullet-}$ (0,0) threshold should be observed at ≈550 nm in the present EPD experiment. Thus, only the $^1A_2$ excited electronic state and the $^3A_2$ ground triplet state of PhN would be observed in our photon energy range of 1.35–2.30 eV (920–540 nm).

Starting at the low-energy end of Figure 1a, the heavy arrow locates the (0,0) transition threshold at 867.9 ± 7 nm (1.429 ± 0.011 eV) from the $^2B_2$ ground state of $PhN^{\bullet-}$ to the $^3A_2$ ground state of PhN (Table I). This threshold agrees well with that of the reported EPD (1.46 ± 0.01 eV)[19,25] and PES (1.446 ± 0.012 eV)[6] studies of $PhN^{\bullet-}$.

The (0,0) threshold is followed by three weaker features that decrease in size with increasing photon energy; the thresholds are marked by the smaller arrows at 834, 803, and 772 nm (Figure 1a).[34] The average spacing between these four thresholds is ≈476 cm^{-1}. These factors suggest that the three features at higher energy than the (0,0) feature are a vibrational progression from the $v = 0$ vibrational state of $^2B_2$ $PhN^{\bullet-}$ to three low-energy excited vibrational states, $v = 1$–3, of $^3A_2$ PhN (Table I). From the table of calculated vibrational frequencies for $^3A_2$ PhN given by Kim et al.,[27] a ring in-plane bending mode (≈500 cm^{-1}), a CH out-of-plane bend or a ring in-plane bend coupled to a ring stretching mode (≈950 cm^{-1}), and the CN stretch (≈1200 cm^{-1}) or a CH in-plane bending mode (≈1400 cm^{-1}) that are both strongly coupled with the ring stretching modes appear to be reasonable vibrations associated with the (1,0)–(3,0) excited states.[35] Travers et al.[6] approximately simulated their PES Franck–Condon profile

(31) The problems with folding together σ_{rel} vs λ data sets from two or more dye runs have been presented and discussed.[10] All necessary precautions and checks were taken to minimize this problem in the present work.

(32) (a) Proctor, A.; Sherwood, P. M. A. *Anal. Chem.* **1982**, *54*, 13. (b) Proctor, A.; Sherwood, P. M. A. *Anal. Chem.* **1980**, *52*, 2315.

(33) Janousek, B. K.; Zimmerman, A. H.; Reed, K. J.; Brauman, J. I. *J. Am. Chem. Soc.* **1978**, *100*, 6142.

(34) The thresholds marked by small arrows in Figure 1a could not have been resolved using the xenon lamp–monochrometer light source with its broad band widths.

(35) The calculated vibrational frequencies have been reduced by 10% since SCF frequencies are typically high by this amount.[27]

Table I. Feature Thresholds and Energy Splittings for EPD of $^2B_2$ PhN$^{\bullet-}$

threshold assign[a]	threshold wavelength,[b] nm	energy,[c] eV (kcal mol^{-1})	ΔE from origin, eV	PES energy,[d] eV
(0,0)	867.9 ± 2	1.429 ± 0.011 (32.95 ± 0.25)		1.446 ± 0.012
(1,0)	834.0 ± 3	1.487 ± 0.013 (34.29 ± 0.30)	0.058 ± 0.017	1.508 ± 0.010
(2,0)	803.3 ± 3	1.544 ± 0.013 (35.61 ± 0.30)	0.115 ± 0.017	1.566 ± 0.014
(3,0)	772.2 ± 3	1.606 ± 0.014 (37.03 ± 0.32)	0.177 ± 0.018	1.623 ± 0.020
(0,2)	598.1 ± 3	2.073 ± 0.024 (47.80 ± 0.55)	0.151 ± 0.037[e]	2.089 ± 0.025
(0,1)	582.1 ± 3	2.130 ± 0.025 (49.12 ± 0.58)	0.094 ± 0.038[e]	2.146 ± 0.025
(0,0)	557.6 ± 3	2.224 ± 0.028 (51.29 ± 0.64)		≈2.20 ± 0.03[f]

[a] The state-to-state transition assignments are those given in the text in agreement with those of Travers et al.[6] [b] The thresholds are determined from the maxima in the second derivatives of the smoothed σ_{rel} vs λ plot (Figure 1b). [c] ±7 nm; see the Results section. [d] Reference 6. [e] Based on the (0,0) threshold at 557 nm. [f] Calculated by adding the average energy separation of 0.058 eV for the PES (0,3)–(0,1) hot bands to the energy of the (0,1) hot band.[6]

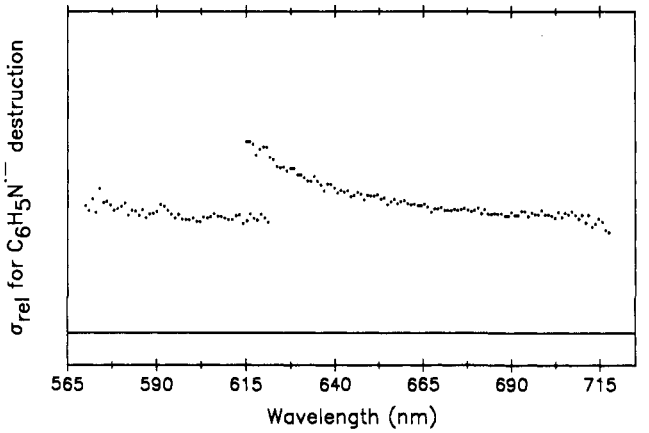

Figure 2. The complete data sets for the Rh6G and DCM dye runs used to construct Figure 1a are shown. These data sets are offset for clarity.

for these same three vibrational states with "a phenyl ring/CN distortion at 1300 cm^{-1} and a ring-breathing vibration at 515 cm^{-1}".

Moving to higher energy, a slow rise in the EPD σ_{rel} is observed between 675 and 620 nm with an apparent peak at 620 nm. The 620-nm peak and the upward curvature between about 685 and 620 nm are artifacts of the folding together of the LDS 722, DCM, and Rh6G data sets due to a small concave bow in the DCM data.[31] This is shown in Figure 2 that includes all of the data points for the Rh6G and DCM runs used to construct Figure 1a. While the overlap at 620 nm in the two dye runs is small, it is clear that *neither data set* indicates a change in slope in this wavelength range although the point scatter is increasing as the intracavity powers of each dye drop off. The bowing of the DCM data set, which is reproduced in all eight data sets obtained with DCM, is not believed to be associated with a specific feature in this overlap region of the EPD spectrum. The cause of the bow is unknown.

At wavelengths <620 nm, two small peaks with λ_{max} at about 590 and 575 nm are apparent in Figure 1a. The thresholds for these two peaks taken from the first and second derivatives of the smoothed data from 620 to 540 nm are at 598.1 ± 3 and 582.1 ± 3 nm, respectively. These peaks are followed by a steep rise in the EPD σ_{rel} at shorter wavelengths with a threshold indicated by the derivatives at 568.6 ± 3 nm as the performance of the Rh110 dye falls off. The feature centered at about 575 nm and the steep rise appear in each of the seven separate runs (photodestruction of PhN$^{\bullet-}$ and appearance of $SF_6^{\bullet-}$) made with Rh110.

The two peaks with thresholds at 598 and 582 nm are, within the error limits, at the same energies as those labeled γ and δ, respectively, by Travers et al.[6] (Table I). These two features "correspond to detachment from hot bands of the ion ($\tilde{a}\ ^1A_1$)-PhN($v'=0$) ← ($\tilde{X}\ ^2B_2$)PhN$^{\bullet-}$($v''=1,2$)".[6] The relative intensities of the these features in Figure 1a centered at about 590 ($v''=2$) and 575 nm ($v''=1$), $I_{v''=2} < I_{v''=1}$, are in accord with this assignment. The energy spacing of 863 cm^{-1} (≈2.5 kcal mol^{-1}) between $v''=0$ and 2 should be about the average 298 K thermal energy of the PhN$^{\bullet-}$ ions. The hot band transition from $v''=3$ of $^2B_2$ PhN$^{\bullet-}$ reported in the PES spectrum[6] was not apparent in this EPD study. The absence of at least one observable hot band transition at wavelengths >868 nm is probably due to the much smaller intensities of the hot bands[6] relative to the already low intensity observed for the $^3A_2$ PhN ← $^2B_2$ PhN$^{\bullet-}$ (0,0) transition.

We believe that the high-energy steep rise in σ_{rel} is part of the low-energy side of the intense (0,0) transition from $^2B_2$ PhN$^{\bullet-}$ to the singlet excited electronic state, $^1A_2$, of PhN. The beginning of this (0,0) threshold region at 568.6 nm, measured from the second derivative in Figure 1b, indicates the presence of transitions from excited rotational states of PhN$^{\bullet-}$. Subtraction of the rotational correction of $1.5kT$ (0.045 eV, 11 nm at this photon energy) places the (0,0) threshold at 557.6 ± 7 nm (2.224 ± 0.028 eV). This threshold is in excellent agreement with that predicted from the data of Travers et al.,[6] ≈2.20 ± 0.03 eV (Table I).

Although the final eight highest-energy data points were obtained with intracavity powers of 8–19 W, the next 20 points leading to the (0,0) threshold had intracavity powers of >20 W. Thus, we are confident that the above determination of the (0,0) threshold at 558 nm is not laser power limited.

The lower intensity observed for the (0,0) transition to $^3A_2$ PhN compared to that of the $^1A_2$ excited state suggests that there is better Franck–Condon overlap between the manifolds of $^2B_2$ PhN$^{\bullet-}$ and $^1A_2$ PhN than between $^2B_2$ PhN$^{\bullet-}$ and $^3A_2$ PhN. In $^2B_2$ PhN$^{\bullet-}$, a $\sigma^1\pi^2$ species,[6] we expect strong delocalization of the electron pair formally on nitrogen into the aromatic ring giving a short C_1N bond with largely double-bond character. π-Delocalization of the $3b_1$ electron in $^1A_2$ PhN will be greater than in $^3A_2$ PhN because of their spin states. The calculated C_1N bond lengths and stretching frequencies in $^1A_2$ PhN (1.274 Å[27] (1.288 Å[28]) and 1855 cm^{-1} [27] indicative of a C=N) and in $^3A_2$ PhN (1.388 Å[27] (1.374 Å[28]) and 1345 cm^{-1} [27]) are in agreement with this interpretation. Therefore, the structures of $^2B_2$ PhN$^{\bullet-}$ and $^1A_2$ PhN should be very similar, leading to better Franck–Condon overlap and more intense EPD transitions.

The present work was well underway when we learned that Professor G. B. Ellison and his group at Colorado were completing studies of PhN$^{\bullet-}$ with PES.[29] Their results[6] are included in the last column in Table I for comparison. The agreement in the threshold energies for the individual features measured in the two experiments is excellent. The Ellison group did not report the value for the $^1A_2$ PhN ← $^2B_2$ PhN$^{\bullet-}$ (0,0) threshold[6] that is estimated in Table I.

Although the weak (0,1)–(0,3) vibrational features appear to be steps superimposed on the photodetachment background, the $^3A_2$ PhN ← $^2B_2$ PhN$^{\bullet-}$ (0,0) transition (γ_{max} 869 nm), the two hot band transitions (λ_{max} 585 (2,0) and 578 nm (1,0)), and the $^1A_2$ PhN ← $^2B_2$ PhN$^{\bullet-}$ (0,0) features appear as distinct peaks. Such features are reminescent of the modestly sharp peaks observed in the EPD spectrum of acetophenone enolate anion where a dipole supported state of the anion lying just below the threshold energy was suggested to be involved.[10,36] Additional experimental results have been reported that argue strongly for excitation of

(36) Zimmerman, A. H.; Brauman, J. I. *J. Chem. Phys.* **1977**, *66*, 5823.

certain anions to vibrational levels of the first excited dipole supported state in other EPD results.[37,38] In such diffuse electronic states, the electron is bound by the dipole of the radical with μ_{min} = 1.625 D for a stationary, fixed dipole[39] or ≈2.1 D for the introduction of rotation into the system.[40] That a related dipole supported state may explain the well-defined features in the present work is the calculated dipole moment of 2.4 D for $^3A_2$ PhN from SCF calculations with a 6–31++G** basis.[29]

The thermodynamic parameters available from these results include the EAs of $^3A_2$ PhN (1.429 ± 0.011 eV; 32.95 ± 0.25 kcal mol^{-1}) and $^1A_2$ PhN (2.224 ± 0.028 eV; 51.29 ± 0.64 kcal mol^{-1}). The difference in these EA values of 0.795 ± 0.030 eV (18.33 ± 0.69 kcal mol^{-1}) is the energy gap separating the ground vibrational levels of these two electronic states of PhN. From $\Delta H°_{f,298}(PhN^{\bullet-})$ = 62.9 ± 4.3 kcal mol^{-1}, the $\Delta H°_{f,298}$ of the two states of PhN are determined. Since the EA is a 0 K parameter, ideally, the $\Delta H°_{f,298}(PhN^{\bullet-})$ would be corrected to 0 K by the difference in the heat capacities in the anion radical at the two temperatures. Addition of the EAs of the states of PhN to $\Delta H°_{f,0}(PhN^{\bullet-})$ would yield the corresponding $\Delta H°_{f,0}(PhN)$ that would then be corrected to 298 K by the difference in the heat capacities of the PhN state at 0 and 298 K. The differences in the heat capacities, $(H_T - H_0)$, of $^3A_2$ and $^1A_2$ PhN from 0 to 298 K are found to be 1.29 and 1.51 kcal mol^{-1}, respectively, from the calculated vibrational frequencies ($\omega \leq 1600$ cm^{-1})[27] and standard tables.[41] While the vibrational frequencies and, thus, the heat capacity changes of $PhN^{\bullet-}$ are unknown, they are reasonably approximated by the frequencies of $^1A_2$ PhN, which is structurally most similar to $^2B_2$ $PhN^{\bullet-}$ as deduced from the relative intensities of the two (0,0) EPD transitions (above). The likely small changes in the frequencies between $PhN^{\bullet-}$ and the two states of PhN are expected to yield $\delta(H_T - H_0)$ of <0.5 kcal mol^{-1}. Since this difference is significantly smaller than the error associated with $\Delta H°_{f,298}(PhN^{\bullet-})$, the corrections are omitted in calculating the heats of formation of the two states of PhN yielding $\Delta H°_{f,298}(^3A_2$ PhN) = 95.9 ± 4.3 kcal mol^{-1} and $\Delta H°_{f,298}(^1A_2$ PhN) = 114.2 ± 4.3 kcal mol^{-1}. $D°(PhN^{\bullet}-H)$ = 91.3 ± 3.8 kcal mol^{-1} is available from the thermodynamic cycle in eq 5 in agreement with the value previously given.[19]

$PhNH^{\bullet} \rightarrow PhN^{\bullet-} + H^+$	$+PA(PhN^{\bullet-})$
$PhN^{\bullet-} \rightarrow PhN^{2\bullet} + e^-$	$+EA(^3A_2$ PhN)
$H^+ + e^- \rightarrow H^{\bullet}$	$-IP(H^{\bullet})$
$PhNH^{\bullet} \rightarrow PhN + H^{\bullet}$	$D°(PhN^{\bullet}-H)$ (5)

Table II. Thermodynamic Values Determined in This Study

species	EA[a]	$\Delta H°_{f,298}$[a]
$^3A_2$ PhN	32.95 ± 0.25	95.9 ± 4.3
$^1A_2$ PhN	51.29 ± 0.64	114.2 ± 4.3
$^2B_2$ $PhN^{\bullet-}$		62.9 ± 4.3[b]

[a] In kcal mol^{-1}. [b] Corrected from that originally given in ref 15.

Summary

This determination of the EPD of $PhN^{\bullet-}$ establishes the EAs of the triplet ground state, $^3A_2$, and the singlet excited state, $^1A_2$, of PhN listed in Table II. From the difference in these two EA values, the singlet–triplet energy gap of 0.795 ± 0.030 eV (18.33 ± 0.69 kcal mol^{-1}) is measured. Addition of the 0 K EAs of these two states of PhN to $\Delta H°_{f,298}(PhN^{\bullet-})$ gives the heats of formation of the two electronic states of PhN (Table II). At this time, experiment and theory are in accord on the magnitude of the energy gap between the ground state and the first excited state of PhN.

Acknowledgment. This research was supported by a grant from the National Science Foundation. We thank Professor Barney Ellison for exchanges of data and information, fruitful discussions, and a preprint. We thank Professor Matt Platz for suggesting this study, Professor Wes Borden for discussions and a preprint, and Professor Donald Setser for his continuing helpful assistance.

(37) (a) Jackson, R. L.; Zimmerman, A. H.; Brauman, J. I. *J. Phys. Chem.* **1979**, *71*, 2088. (b) Wetmore, R. W.; Schaefer, H. F.; Hiberty, P. C.; Brauman, J. I. *J. Am. Chem. Soc.* **1980**, *102*, 5470.

(38) Marks, J.; Comita, P. B.; Brauman, J. I. *J. Am. Chem. Soc.* **1985**, *107*, 3718.

(39) (a) Turner, J. E.; Fox. K. *Phys. Lett.* **1966**, *23*, 547. (b) Crawford, O.; Dalgarno, A. *Chem. Phys. Lett.* **1967**, *1*, 23. (c) Crawford, O. H. *Proc. Phys. Soc., London* **1967**, *91*, 279.

(40) (a) Garrett, W. R. *Chem. Phys. Lett.* **1970**, *5*, 393. (b) Garrett, W. R. *Phys. Rev. A* **1971**, *3*, 961. (c) Crawford, O. H.; Garrett, W. R. *J. Chem. Phys.* **1977**, *66*, 4968.

(41) Pitzer, K. S. *Quantum Chemistry*; Prentice-Hall: Englewood Cliffs, NJ, 1953; Appendix 13.